THE JOURNAL OF PHYSICAL CHEMISTRY C
A JOURNAL OF THE AMERICAN CHEMICAL SOCIETY

pubs.acs.org/JPCC

Article

Tunable Dielectric Switching of (Quinuclidinium)[$MnCl_4$] Hybrid Compounds

Natalia A. Wojcik, Dorota A. Kowalska, Monika Trzebiatowska, Ewelina Jach, Adam Ostrowski, Waldemar Bednarski, Marek Gusowski, Piotr Staniorowski, and Agnieszka Cizman*

Cite This: *J. Phys. Chem. C* 2021, 125, 16810−16818

Read Online

ACCESS | Metrics & More | Article Recommendations | Supporting Information

ABSTRACT: Inorganic−organic hybrid QMnCl (Q = quinuclidinium) crystals were synthesized and characterized. The X-ray and variable-temperature IR/Raman analysis demonstrate that the crystals undergo a reversible structural phase transition, which originates from an order−disorder process and is related to the dynamics of the organic Q cation. Dielectric function measurements disclose a switchability between low ("OFF") and high ("ON") dielectric states centered at around 285 K. Owing to a remarkable temperature-dependent dielectric function, this type of molecular compound can represent an interesting tunable and switchable dielectric material for a diverse range of applications.

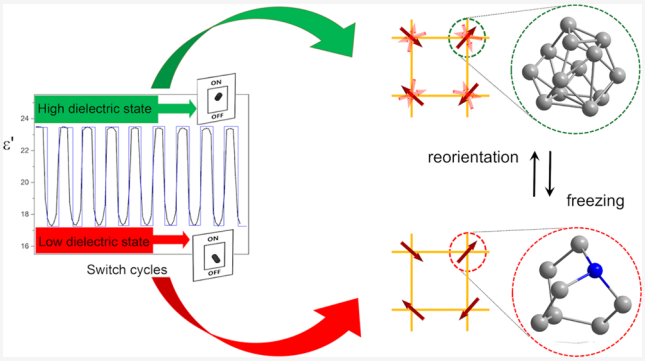

1. INTRODUCTION

The research into hybrid organic−inorganic compounds (HOICs) has rapidly evolved in recent years.[1] The past decade has seen an evaluation of scientific understanding and capabilities of HOIC materials architecture whose properties are controlled by both organic and inorganic components in the structure. The scientific purposes concern a characterization of the physicochemical properties of functional materials from HOICs, as these materials have received an exceptional attention due to interesting electric,[2] optical,[3−5] and magnetic[6] properties. It is known that the multifunctional properties of HOICs, e.g. dielectric switching behavior,[7−9] ferroelectric[10−12] properties, or multiferroicity,[13,14] are mainly determined by hydrogen bonding. Importantly, switchable dielectric materials which show a conversion between high and low-dielectric states are promising as integral elements of electrical and electronic devices, including phase shifters, varactors, data communication, and rewritable optical data storage. Moreover, molecular electrical switches with "ON−OFF" mode belong to a highly desirable class of intelligent materials due to their sensitive responses. Generally, in molecular compounds, a dielectric response has three microscopic origins such as dipolar reorientation, ionic displacement, and electronic polarization.[15,16] At high temperatures (HT), above phase transition (PT), the dipolar reorientation has the greatest contribution to the dielectric function, corresponding to the high-dielectric states ("ON"), while below PT temperature, when reorientations are frozen, low-dielectric state ("OFF") appears. Therefore, changes in ordering of ions or polar molecules affect the switchable dielectric properties between disordered and frozen states. Most of the synthesized hybrid crystals undergo reversible structural PTs. It is found that both order−disorder transformations of polar organic cations and weak displacements of inorganic frameworks make contributions to its switchable dielectric properties.[17,18] Particularly, recent scientific reports have revealed that for hybrids with spherical molecules[19] such as dabco (1,4-diazabicyclo[2.2.2]octanium) or Q (quinuclidinium), a dynamic rotation or reorientation freezing involves interesting physicochemical properties and structural PT.[20,21] The search for good switchable dielectric materials is nontrivial, mainly due to satisfying simultaneously different requirements, e.g., attractive working temperature, sharp steplike phase transition, small-frequency dependence as well as easy and profitable technology.

2. EXPERIMENTAL PROCEDURES

Manganese(II) chloride and quinuclidine (Q) were purchased from commercial sources and used without any further purification. Quinuclidine (0.219 g) and $MnCl_2{\cdot}4H_2O$ (0.781 g) were mixed in an acidic aqueous solution (50 mL), wherein the total amount of used 37% HCl acid was about 8 mL. After few weeks, during which the solvent was allowed to slowly

Received: May 24, 2021
Revised: July 14, 2021
Published: July 28, 2021

https://doi.org/10.1021/acs.jpcc.1c04545
J. Phys. Chem. C 2021, 125, 16810−16818

Table 1. Experimental Details for QMnCl[a]

	phase I	phase II
	Crystal Data	
chemical formula	$Cl_4Mn{\cdot}2(C_7H_{14}N)$	$Cl_4Mn{\cdot}2(C_7H_{14}N)544$
M_r	421.16	421.16
crystal system space group	orthorhombic *Pnma* (no. 62)	monoclinic *P*21/*c* (no. 14)
temperature (K)	295	260
a, *b*, *c* (Å)	12.718(5), 9.550(4), 16.468(7)	9.366(4),16.785(7), 12.545(5)
α, β, γ (deg)	90, 90, 90	90, 92.96(2), 90
V (Å^3)	2000.2(14)	1969.5(14)
Z	4	4
μ (mm^{-1})	1.18	1.21
crystal size (mm)	0.29 × 0.23 × 0.14	
	Data Collection	
T_{min}, T_{max}	0.796, 1.000	0.986, 1.000
no. of refl. measured, independ., obs. [$I > 2\sigma(I)$]	14430, 2636, 1319	7212, 7212, 3912
R_{int}	0.025	0.052
$(\sin\theta/\lambda)_{max}$ (Å^{-1})	0.689	0.691
	Refinement	
$R[F^2 > 2\sigma(F^2)]$, $wR(F^2)$, *S*	0.113, 0.417, 1.42	0.055, 0.171, 0.95
absorption correction	multiscan	multiscan
no. of reflections	2636	7212
no. of parameters	92	218
no. of restraints	0	61
H atoms treatment	H-atom parameters not defined	H-atom parameters constrained
$\Delta\rho_{max}$, $\Delta\rho_{min}$ (e Å^{-3})	0.70, −0.92	0.62, −0.49
twin refinement		refined as a 2-comp. twin
twin refinement parameter		0.5082(16)

[a]Crystal structures at 260 and 295 K have been deposited with numbers CCDC 2094455−2094456.

evaporate at room temperature, the crystals of $Cl_4Mn_2(C_7H_{14}N)$ (**QMnCl**) were obtained in 73% yield (based on $MnCl_2{\cdot}4H_2O$).

The single-crystal X-ray diffraction experiments were performed on an Oxford X'Calibur four-circle single-crystal diffractometer equipped with a CCD camera using graphite-monochromated Mo Kα radiation (λ = 0.71073 Å) generated at 50 kV and 22 mA. The Oxford heating−cooling device was used to maintain nonambient temperatures. For data collection and reduction, the program CrysAlis PRO 1.171.38.46[22] was involved. Empirical absorption was amended using spherical harmonics, implemented in SCALE3 ABSPACK scaling algorithm. The crystal structures, at 295 and 260 K, were solved by direct methods and refined by the full-matrix least-squares methods on F2 utilizing SHELX-2014 crystallographic software package.[23] Olex2[24] was the software used to prepare material for publication. The Diamond[25] program was used to create the graphic representations of the crystal structure. All nonhydrogen atoms, which were not disordered, were refined anisotropically. C-bound and N-bound H atoms, from ordered cations, were constrained to ride on their parent atoms (instructions AFIX 13 and AFIX 23 in SHELXL-2014).[23] The crystal data together with experimental and refinement details for all phases are presented in Table 1. The phase purity of the bulk sample was checked by powder X-ray diffraction (PXRD) and shown in the SI (Figure S6a). PXRD data were collected with a PANalytical X'Pert diffractometer equipped with a PIXcel solid-state linear detector using Cu Kα radiation in a reflection mode.

2.1. IR and Raman Spectroscopy. The temperature-dependent infrared spectra were measured in a heating mode on KBr pellet in the range of 4000−550 cm^{-1} using a Nicolet iN10 Fourier transform IR spectroscopy microscope equipped with a ZnSe-Linkam cryostat cell THMS600 with a temperature stability of 0.1 K, liquid nitrogen (LN_2)-cooled mercury−cadmium−telluride detector, permanently aligned 15× objective, and 0.7 numerical aperture with working distance set at 16 mm. The Raman spectra were measured in a heating mode using a Renishaw InVia Raman spectrometer equipped with a confocal DM 2500 Leica optical microscope, a thermoelectrically cooled CCD as a detector, and a diode laser operating at 830 nm, which has allowed the measurements within 50−2000 cm^{-1}. The use of other excitation sources was impossible due to strong luminescence. The spectral resolution in IR and Raman experiments was set at 2 cm^{-1}.

Thermal properties were performed by the heating and cooling of the weighed and hermetically sealed in Al pans samples with the use of a Mettler Toledo DSC instrument. The measurements were done in the temperature range of 260−330 K and with heating rates of 5 K min^{-1} and under a nitrogen atmosphere.

EPR measurements were performed using a X-band ELEXSYS (Bruker) spectrometer equipped with an ER 4102ST resonator. The temperature was stabilized (±0.1 K) by ER4131RT controller.

The complex dielectric permittivity ($\varepsilon = \varepsilon' - i\varepsilon''$) was performed by the Novocontrol Alpha Impedance Analyzer in the frequency range of 1 Hz to 1 MHz with an applied AC voltage of 1 V. The temperature dependencies of the dielectric permittivity of polycrystalline samples, using silver-painted electrodes, were measured between 350 and 250 K with the temperature step 2 K and controlled using the nitrogen gas cryostat with stability better than 0.1 K. Additionally, switching

https://doi.org/10.1021/acs.jpcc.1c04545
J. Phys. Chem. C 2021, 125, 16810−16818

of dielectric permittivity was tested around the phase transition at a temperature range of 295−272 K more than 10 times.

3. RESULTS AND DISCUSSION

3.1. Thermal Properties. In **QMnCl**, in the temperature range of 260−330 K, a well-defined pair of exo-/endo-thermal anomalies appears at 279/289 K during the cooling/heating cycle, respectively (Figure 1).

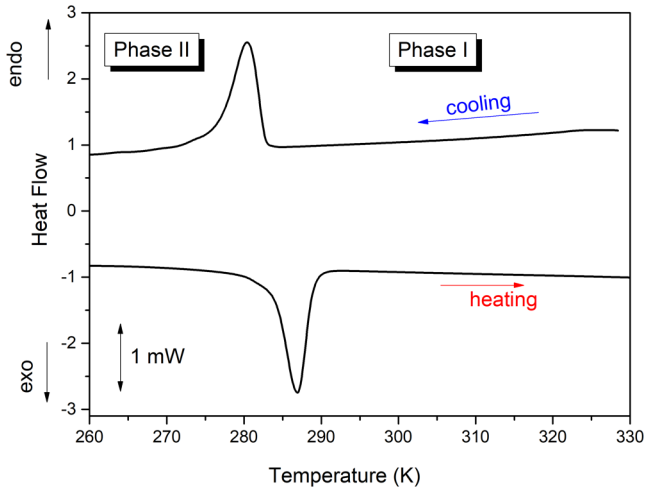

Figure 1. DSC curves of the **QMnCl** sample in the cooling−heating cycle.

The sharp character of PT as well as a large thermal hysteresis (~10 K) of the peaks at around 285 K indicates a discontinuous first-order phase transition type. The average entropy changes, ΔS (SI, Figure S1), were extracted from the specific heat curve (SI, Figure S2) with the value of 10 J mol^{-1} K^{-1}. The extent of disorder in Phase I was specified using the Boltzmann equation $\Delta S = R\ln(N)$, where R is the gas constant and N is the number of disordered sites. The value of N, calculated to be 3.35, suggests a disorder in the high-temperature (HT) Phase I.

3.2. Crystal Structure. Two structurally distinguishable phases (Phase I and Phase II) of **QMnCl** have been characterized by single-crystal X-ray diffraction measurements. The crystal data together with experimental and refinement details are given in Table 1.

Phase I: Phase I of **QMnCl**, measured at 293 K, has an orthorhombic symmetry with the centrosymmetric *Pnma* (no. 62) space group. An isolated $MnCl_4^-$ tetrahedron constitutes the inorganic part of the structure. Together with two Q ions, they create the independent part of the structure (Figure 2a).

In this phase, a significant disorder of both Q ions is observed (SI, Table S1). Therefore, it was not possible to designate the exact positions of disordered species (SI, Figure S3). In the structure model, Q cations are disordered to such degree that atoms belonging to those ions have isotropic temperature factors high enough to implicate a larger number of possible positions that result from structural sites and suggest potential movements in their cavities. In the single unit cell, isolated $MnCl_4^-$ tetrahedrons are arranged in two layers. Two Mn tetrahedrons are below and two above planes with c = 0 and c = 1/2. Among them, there are two symmetrically distinguishable Q cations located, multiplied by symmetry operations inherent to the corresponding phase (marked with light yellow and blue colors in Figure 2c). One of the Q cations (marked light yellow, Figure 2c) is aligned alternatively with $MnCl_4^-$ tetrahedra in two axis directions, a and c. The other group of Q cations (marked light blue, Figure 2c) are shifted away from the lines created by $MnCl_4^-$ tetrahedra on the ac planes, slightly in a-axis and significantly in the c-axis direction. The differences in the arrangement of cations cause the variations of Q cation disorder in the **QMnCl**. For the first Q cation, two positions can be distinguished (Figure 2a). The other Q cation is disordered over a greater number of sites, which can be divided at least into four. However, high isotropic temperature factors of both Q ions suggest a higher degree of disorder, probably dynamic.

Phase II: In Phase II, **QMnCl** has a monoclinic symmetry and accommodates the $P21/c$ (no. 14) space group. The change of crystal axes is as follows: $a_{II} = b_I$, $b_{II} = c_I$, and $c_{II} = a_I$. The content of the asymmetric unit is the same as in Phase I (Figures 2b and S5b,c). One of the Q ions is ordered, whereas the other one is disordered over three positions with the refined occupancy factors equal to 0.39, 0.29, and 0.32 (see Table S2 and Figure 2d having red, yellow, and green color, respectively). In Figure 2b, atoms belonging to one of three disordered positions of Q ion are labeled with letters A, B, and C and are presented in three shades of gray and blue for C and N atoms, respectively. The net of weak hydrogen bonds connects Q ions to Mn tetrahedrons belonging to one of the two layers (SI, Figures S4 and S5d). In Table S4 (SI), possible hydrogen N−H···Cl bonds are listed. Additionally, in Phase II, all of the distances between Mn and Cl atoms are longer than corresponding distances in Phase I (see SI, Tables S4 and S5). This phenomenon is probably caused by an elongation of the longest lattice parameter when the temperature is being lowered. Figure S6b (SI) presents changes of a, b, and c lattice parameters with the temperature.

3.3. IR and Raman Spectroscopic Studies. Vibrational spectroscopy provides a valuable insight into the interactions and allows to study the dynamic effects during PT. The temperature-dependent IR and Raman spectra of **QMnCl** crystal are presented in Figures S7−S9 (SI), respectively. The observed modes originate from internal vibrations of the organic cation, Mn−chloride tetrahedra, as well as lattice modes.

Table S6 presents a factor group analysis done for the compound. The observed IR and Raman wavenumbers, along with the assignment, are given in Table S7 (SI). The symbols used in the text have been explained in the footnote of this table. The assignment is based mostly on the data available for the compounds containing quinuclidinium and similar cations (e.g., dabco) or other ethylene-containing amines and manganese halides.[26−29] Here, we will focus on some features of the spectra and on the effect of temperature. Basically, since the compound is centrosymmetric in both phases, one should observe asymmetric modes in IR and symmetric modes in Raman spectra, respectively. Table S6 gives the factor group analysis for $MnCl_4$ moieties (due to the disorder of Q cations, their analysis is omitted here). In a perfect scenario, the tetrahedra might be regarded as having T_d symmetry which are placed in a general position (C_1) at Phase II and mirror plane (C_s) at HT, leading to a reduced number of active modes in Phase I compared to Phase II. The onset of the phase transition both in IR and Raman spectra appears at ca. 270/280 K upon heating. The broad bands with the center of gravity in roughly 3430−3360 cm^{-1} range (IR) are assigned to

https://doi.org/10.1021/acs.jpcc.1c04545
J. Phys. Chem. C 2021, 125, 16810−16818

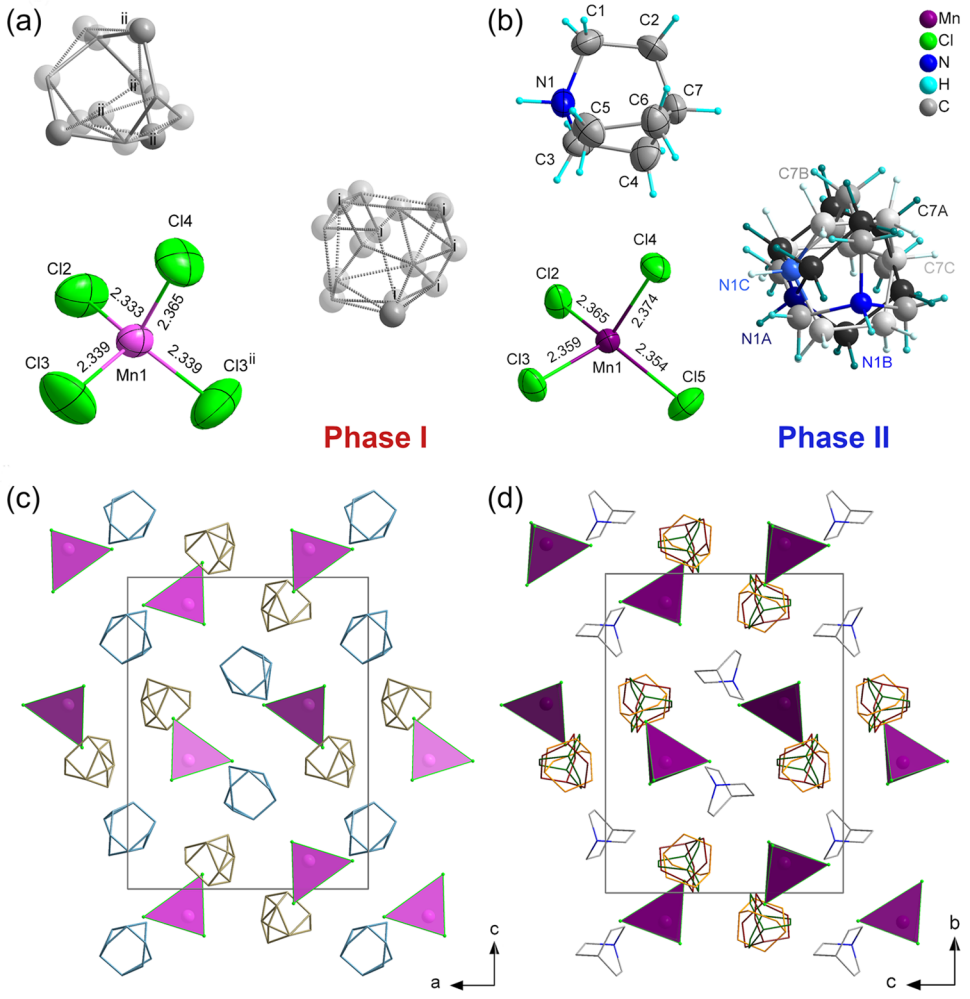

Figure 2. Comparison of the asymmetric units of **QMnCl** in Phase I (a) and Phase II (b), showing the atom numbering scheme together with parts that complete the chemical formula. Atoms are shown in ellipsoid representation at 40% probability level, except atoms belonging to the disordered Q ions, which are shown in standard representation. The partially occupied sites in Phase I are shown as transparent. [Symmetry codes: (i) $x, -y + 3/2, z$; (ii) $x, -y + 1/2, z$]. The view at the crystal structure in Phase I (c) and in Phase II (d). The phases are presented in standard settings of the space groups, and the change of the axes is as follows: $a_{II} = b_I$, $b_{II} = c_I$, and $c_{II} = a_I$.

the stretching vibrations of NH groups of Q cations (Figures S7 and S8). The positions of the bands indicate that one should regard the formed N−H···Cl hydrogen bonding rather as a medium according to the Steiner.[30] This is in agreement with the crystallographic data. The bands broaden insignificantly along temperature increase meaning that the disorder observed in the crystal by X-ray diffraction is very strong already at low temperatures. The wavenumber shifts equal to a few cm^{-1} are low compared to dabcoCrCl[17] crystal and much lower than in other systems undergoing order−disorder processes. For example, in the formamidinium−metal−cyanide complex, the shift has valued almost 50 cm^{-1}.[26] This means that the bond lengths do not vary too much over PT, and this is an evidence of a rotation around the main C_3 axis of the molecule. The NH in-plane and out-of-plane deformation vibrations, found at 1600 and 900−830 cm^{-1}, respectively, are slightly more affected by the temperature than the stretching modes. They influence skeletal stretching modes, as clearly observed by the shift of Raman band at 790 cm^{-1} reaching approximately 6 cm^{-1} for the Raman band at 790 cm^{-1} (Figure 3a). Though here again, the full width at half-maximum (FWHM) does not change dramatically through the PT point, it rather grows steadily within the given temperature range with a small indent at PT. This is consistent with the behavior of NH stretching modes, proving the constant reorientation of quinuclidinium cations. The bands found within 3050−2950 and 1490−1190 cm^{-1} belong to C−H/CH_2 stretching modes and deformation vibrations, respectively, and they are typical of the Q, dabco cation, and other ethylene-containing molecules.[28−31] However, in this case, they are broad (specifically the band at 3050 cm^{-1}) and do not split remarkably even at 80 K (Figure S8). The bending modes observed at 1492 cm^{-1} (δCH_2, IR, RT) and 1342 cm^{-1} (ωCH_2, IR, RT) behave in a similar manner—the wavenumber and FWHM change goes on almost steadily with a small jump around PT, as shown in Figure 3c,d, respectively. This agrees well with the fact deduced from the behavior of NH modes, namely, the presence of disorder well below PT. The bands shift and broaden insignificantly as the temperature rises. This is somewhat similar to what has been observed in the dabcoCrCl crystal;[17] however, the Phase II disorder is much better pronounced in **QMnCl**. An analogous thermal behavior has been found in a metal−organic compound with dabco molecules in the cavities where they rotate freely.[29] The lattice modes observed in Raman spectra below 500 cm^{-1} are the best marker of the PT in this case since they originate from the

https://doi.org/10.1021/acs.jpcc.1c04545
J. Phys. Chem. C 2021, 125, 16810−16818

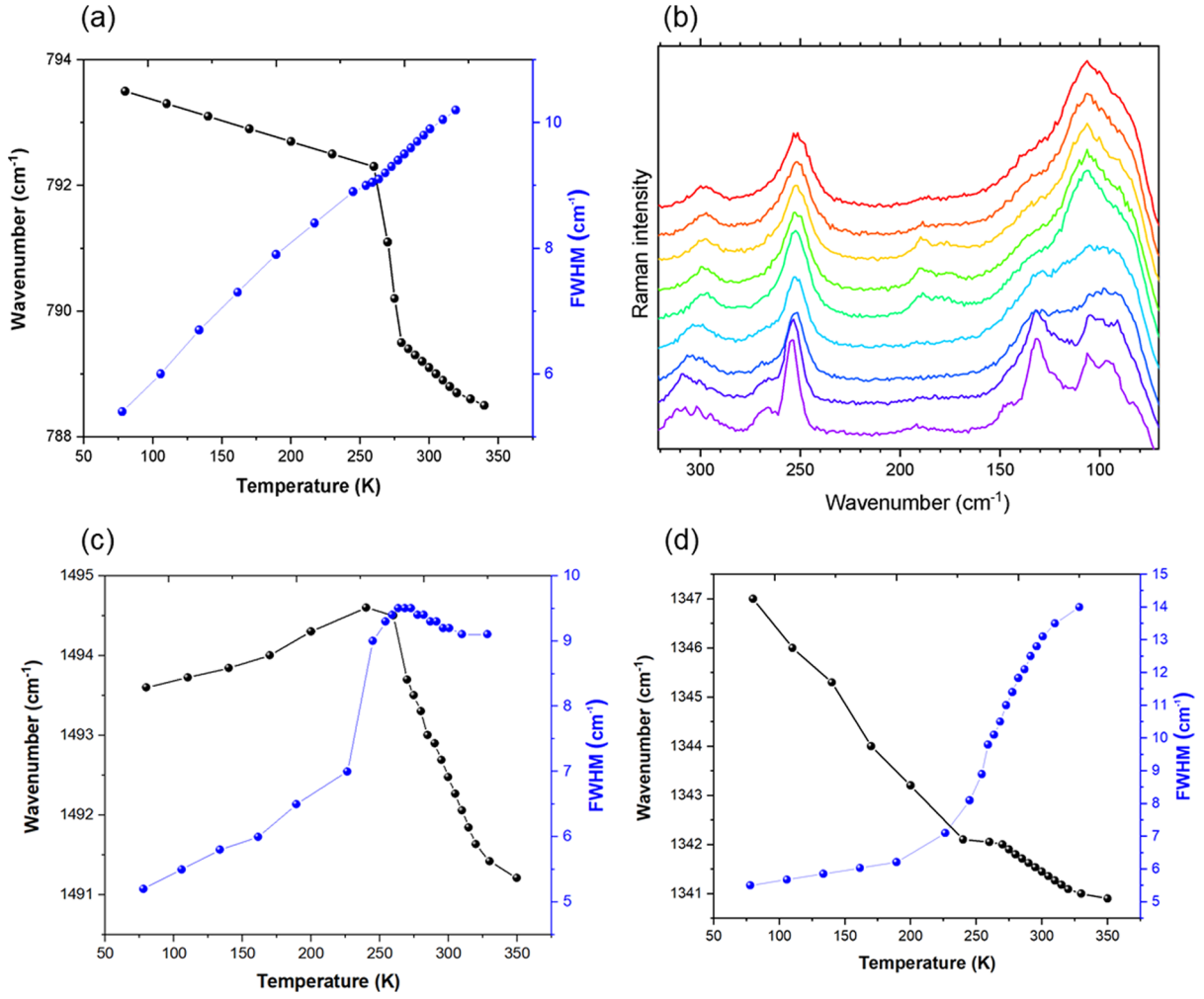

Figure 3. (a) Corresponding wavenumber (black) and FWHM changes (blue) of the Raman band at 790 cm^{-1}; (b) thermal evolution of Raman bands assigned to $MnCl_4$ modes and translations/librations of Q cations; (c) wavenumber (black) and FWHM changes (blue) of the IR band at 1492 cm^{-1}; and (d) wavenumber (black) and FWHM changes (blue) of the IR band at 1435 cm^{-1}.

translation and librations of the whole organic cations and the modes of $MnCl_4$ tetrahedra. The significant changes are found in the case of the band at ca. 300 cm^{-1}, which shifts by 7 cm^{-1} (Figure 3b) while crossing the PT point and subsequently becomes broader. This is associated with the width gain of the band at ca. 250 cm^{-1} and finally with the most remarkable changes observed at 160−80 cm^{-1} (Figure 3b). The latter region faces the merging of two main bands at ca. 130 and 100 cm^{-1} before PT into one broad band upon heating. Taking into account the fact that around 100 cm^{-1} the deformation modes of $MnCl_4$ are active and that the number of the modes stays the same for both phases, we have concluded that the changes are associated with the librations (rotations) of Q cations. This would correspond to the symmetry change of the Q molecule from C_3 into a higher $C_{\infty v}$, meaning basically free rotation and disappearance of some bands. Unlike in dabcoCrCl compound, here the Q cation provides only one N atom for possible hydrogen bonding with the inorganic net; thus, its motions are less constrained than its dabco relative, and it is more likely to take the opportunity to move around. Therefore, it is hereby concluded that the phase transition is caused by the rotation of the whole Q molecule.

3.4. Electrical Properties. The dielectric response to changes in the dynamics mobility of the organic elements during the solid-to-solid phase transition has been studied. Variable-temperature dielectric spectra were performed on the pressed pellet samples of **QMnCl** (Figure 4). The dielectric constant (ε') of complex dielectric shows a sharp steplike anomaly upon the heating and cooling process around 285 K. Below 285 K, at Phase II, ε' remains relatively stable, proving an ordered phase of crystal above the phase transition. Above 285 K, in Phase I, ε' increases with temperature, indicating a disturbance of thermal fluctuation and polarization. It is commonly known that both structural changes and thermally activated molecular rotations under the external electric field are revealed in the behavior of ε'. The visible steplike behavior of dielectric permittivity (Figure 4a) indicates the order−disorder transition, which is mainly attributed to organic cations. In the high-temperature phase (Phase I), Q cations are highly disordered, while in the low-temperature phase (Phase II), their mobility is frozen. Additionally, dielectrics loss, tan δ (Figure 4b), displays small steplike changes around PT temperature at a selected frequency.

The repetition of bistable state cycle measurement between high ("ON") and low ("OFF") dielectric state has been performed to demonstrate the switching behavior of the **QMnCl** sample (Figure 4c). The measurements of dielectric constant at selected frequency and with simultaneous periodic

https://doi.org/10.1021/acs.jpcc.1c04545
J. Phys. Chem. C 2021, 125, 16810−16818

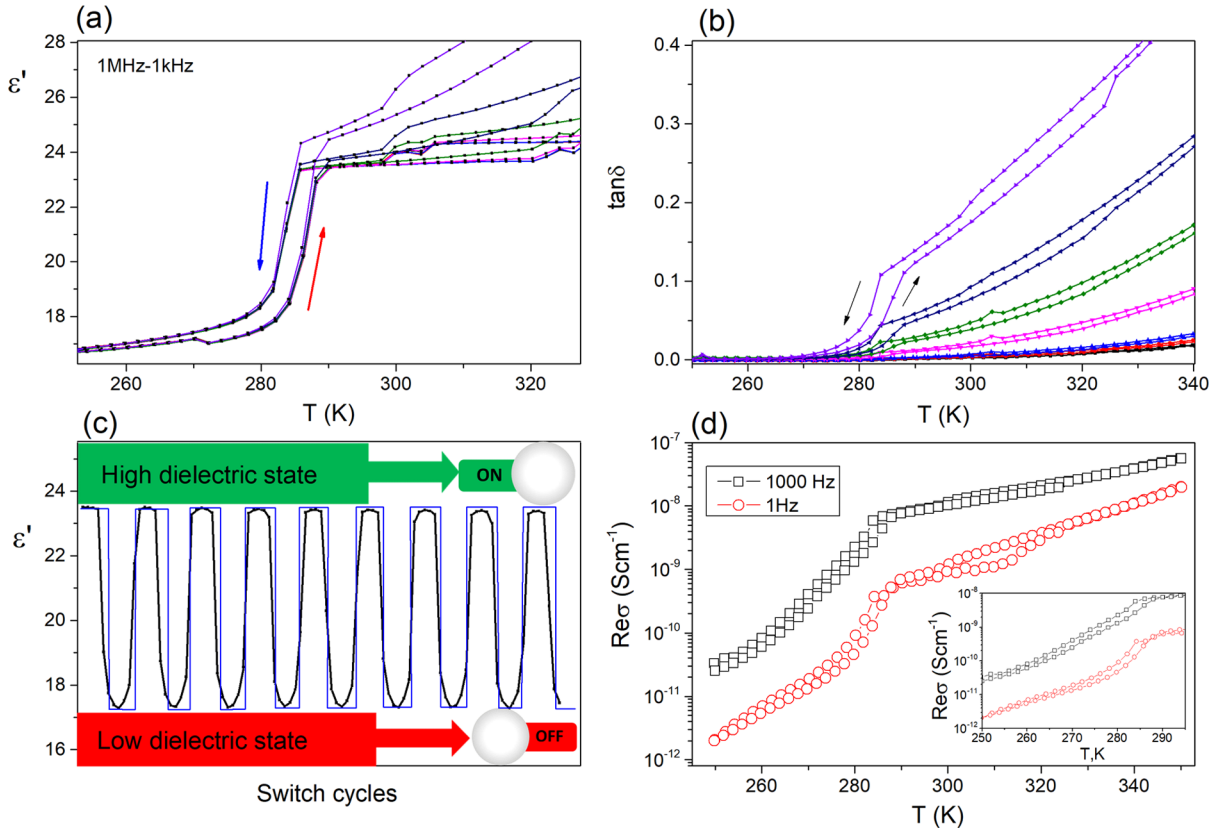

Figure 4. Temperature dependence of (a) the real part of dielectric constant (ε'), (b) dielectric loss ($\tan\delta$) of the **QMnCl** measured at selected frequencies, (c) ε'-switching of the powder pressed pellets of **QMnCl** at 1 MHz recorded after at least nine ON/OFF cycles, and (d) the real part of A.C. conductivity (in log scale) as a function of temperature for selected frequencies. The inset shows the approximation around PT temperature.

temperature changes have been repeated several times. An abscissa indicates the test time, which is correlated with the cycle of the temperature. The blue line is the switching guide to the eye. It is shown that in a high-dielectric state (Phase I), dielectric permittivity ε' after several cycles maintains an almost constant value of 23.5. The rapid decrease in ε' from 23.5 to 17 corresponds to the low-dielectric state (Phase II). Generally, the behavior of switching of dielectric constant can be characterized as a rapid switchable (nearly no-time response) and with some nonzero delay time.[32,33] The rapid switchable materials show rapid system response during the switch ON/OFF process. With the temperature decrease, the rapid response of **QMnCl** from high-dielectric state (ON) to low-dielectric state (OFF) indicates a nearly no-time delay process. In the experiment, one single switching (ON/OFF) circle to finish took about 8−12 min with the speed of dielectric response of around 13 K. This behavior is extremely important due to the application of these compounds as intelligent materials that show a quick response to an external factor and can realize the ON/OFF switching process. Moreover, if one compares the stability of dielectric constant of **QMnCl** after several cycles to other hybrid materials, e.g., MACr,[34] it can be concluded that this material can be considered as an attractive material for electronics devices. Figure 4d shows the temperature dependence of the real part of A.C. conductivity for the **QMnCl** sample at two selected frequencies. The conductivity values are obtained during heating and cooling cycles as marked by arrows. During the heating cycle, the conductivity of the **QMnCl** sample increases with temperature. The increased rate of conductivity with temperature slows down above 290 K what is clearly visible at higher frequency (black curve in Figure 4d). Above 290 K, the conductivity also shows a monotonic increase. This temperature is correlated with the phase transition of **QMnCl**. In the inset, the A.C. conductivity is displayed in a limited scope of temperatures to highlight the effect of PT on the conductivity behavior. It can be seen that around the temperature of phase transition, there is a jump in conductivity which is especially visible at a lower frequency (red curve in Figure 4d). The PT is additionally noticeable as temperature hysteresis in a range from 270 to 290 K during heating and cooling. The increase in conductivity with temperature is typical for ionic semiconductors and is associated with the increased disorder in the material and with increasing proton transport in Q.[35] The Nyquist plots (the imaginary part vs real part of impedance, SI, Figure S10) consist of two overlapping semicircles and the onset of a third one (visible above 300 K), which correspond to three relaxation processes.[36] The third process significantly deviates from the one observed during heating (pink curve) and the one during cooling (blue curve). An analysis of complex impedance may allow combining the electrical parameters with the microstructure of material and separate different conduction mechanisms. The first two relaxation processes were modeled with the use of different empirical relations, and the best fitting results to experimental data were obtained for the superposition of two Cole−Cole relaxation processes. The impedance Cole−Cole relation depicts an equivalent circuit consisting of a resistance and a CPE element

https://doi.org/10.1021/acs.jpcc.1c04545
J. Phys. Chem. C 2021, 125, 16810−16818

connected parallel and can be written as: $Z^* = R(1 + j\omega\tau)\alpha^{-1}$, where Z^* is the complex impedance, R is the equivalent resistance of process, τ is the mean dielectric relaxation time, ω is an angular frequency, and α is a parameter that describes the width of the relaxation time distribution.[36] In the case of our results, two Cole−Cole relations were connected in series to separate the components of the conductivity processes (see the inset in the SI, Figure S10). The fitting analysis was performed in 304−350 K range for both increasing and decreasing cycles. Below 304 K, the second process was observed only as a part of the semicircle and highly overlapped with the beginning of the third process. Therefore, the correct fitting of the process resistance was difficult. The fitting result of two Cole−Cole relations to experimental data is presented for 320 K during the heating and cooling cycles (SI, inset in Figure S10). It can be seen that the fitting curve is in a good agreement with the experimental data for the first two processes (in high- and middle-frequency ranges).

The obtained resistances of two conduction processes have been recalculated to conductivities (based on a sample and electrodes sizes) and are displayed as a function of reciprocal temperature in Figure 5a. The results found for heating and cooling cycles are similar. The first conduction process observed in the high-frequency range exhibits higher conductivity values and lower activation energy compared to the second conduction process observed in the middle-frequency range. Two conduction processes are correlated with proton transfer in Q and Cl^- ion transfer.[35] The beginning of the third process visible at a low-frequency range and high temperatures can be correlated with electrode effects.[37] The relaxation properties of **QMnCl** are discussed based on the complex electrical modulus ($M^* = M' + iM''$) examination. A typical behavior for the relaxation process of the temperature dependence of the imaginary part of the electrical modulus (M'') recorded at various temperatures for **QMnCl** is exposed (SI, Figure S11). A thermally activated process is disclosed by the M'' peaks shifting toward higher frequencies with increasing temperature. The temperature dependence of mean expectation time ($\tau = \tau_0 e^{E_A/kT}$) for a fluctuation energy E_A is shown in Figure 5b. The best least-square fits expose changes in activation energy of dielectric processes resulting from temperature changes (Figure 5b). Below PT temperature, the anion becomes ordered. The order−disorder phenomenon of the carbon atoms of Q and the hydrogen atoms attached to them are assumed to be the main cause of the dielectric response in **QMnCl**. Such disordering exerts a predominant influence on the thermal dynamics of Q and suggests that **QMnCl** can be a potential switchable dielectric material.

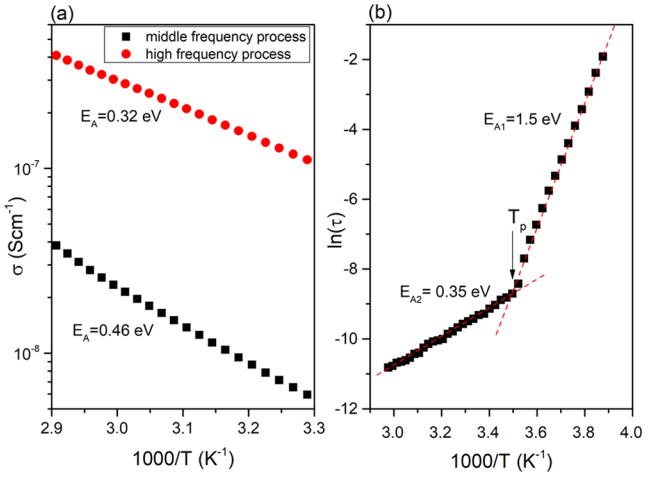

Figure 5. (a) Conductivity vs reciprocal temperature obtained for two relaxation processes from Cole−Cole relations fit (SI, Figure S10). (b) Variable-temperature dependence of relaxation time.

3.5. EPR Study. The EPR spectra of powdered **QMnCl** (presented in Figure 6) consist of a strong line with g-factor g = 2.01 and very weak satellite lines from fine structure, clearly visible at Phase II. In some cases, a strong dipole broadening and/or exchange interaction between Mn^{2+} ($S = 5/2$, $I = 5/2$) ions may smear the fine structure and EPR spectra consist of only a single line, as shown before.[38,39] On the other hand, if the symmetry of the Mn-coordinating environment is not high and the dipole broadening is small enough, a fine structure can still be observed.[40] The last case corresponds to our EPR studies and is consistent with the X-ray data (Figure 3). However, the dipole broadening for individual lines is sufficient to smear the sextet ($2I + 1$) of hyperfine structure.

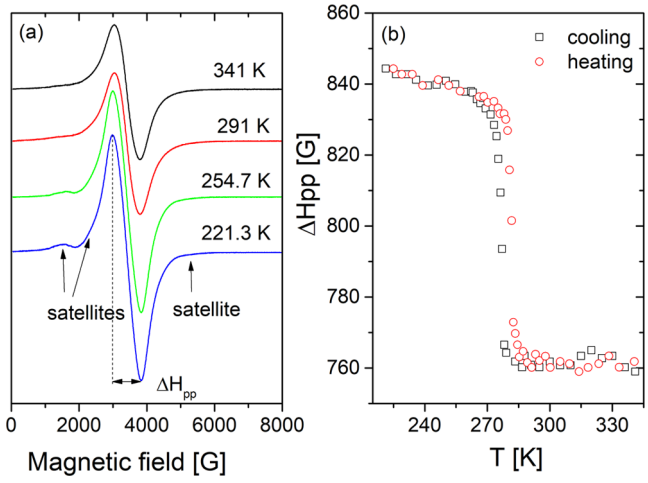

Figure 6. (a) EPR spectra of powdered **QMnCl** for selected temperatures and (b) line width ΔH_{pp} dependence for heating and cooling cycle.

At high temperature, the line width remains almost constant and increases rapidly with temperature decreasing at transition to Phase II. Such line width behavior indicates the first-order PT. Moreover, ΔH_{pp} shows hysteresis, consistent with DSC measurements. From the structural data, one can eliminate the idea that a dipole broadening is the main contribution to the rapid line width decreasing at the PT II → I because the distances between Mn ions change only slightly (Figure S12, SI). It should also be noted that some distances between the nearest Mn^{2+} ions increase and other decrease at PT, which eliminates large changes in a line broadening. Based on structural data (large Mn^{2+}−Mn^{2+} distances) any influence of direct exchange on line width narrowing should be excluded. Therefore, the most probable mechanism responsible for line width decrease at II → I phase transition is averaging out of the anisotropic spin environment triggered by movements.[41−43] This statement is strongly supported by the structural changes that take place during PT because in Phase II, in contrast to HT Phase I, one of the Q ions is disordered and appears in three different orientations.

https://doi.org/10.1021/acs.jpcc.1c04545
J. Phys. Chem. C 2021, 125, 16810−16818

4. SUMMARY

In summary, new organic−inorganic hybrid (quinuclidinium)-$MnCl_4$ is found to show the temperature-induced switchable dielectric permittivity at around 285 K. For obtained materials, an almost unchanged amplitude of dielectric permittivity has been recorded during a few cycles of ON/OFF switching, indicating that a dielectric switching remains both reversible and stable. The detailed analysis of the crystal structure and vibrational spectroscopy indicates that its switchable properties originate from the order−disorder induced by the rotation of Q ions. This material can be used as a potential material for electrically switchable devices or in electronic materials.

■ ASSOCIATED CONTENT

Supporting Information

The Supporting Information is available free of charge at https://pubs.acs.org/doi/10.1021/acs.jpcc.1c04545.

Structural and IR/Raman details as well as electrical results (PDF)

■ AUTHOR INFORMATION

Corresponding Author

Agnieszka Cizman − *Department of Experimental Physics, Wrocław University of Science and Technology, 50-370 Wrocław, Poland;* orcid.org/0000-0002-8906-4080; Email: agnieszka.cizman@pwr.edu.pl

Authors

Natalia A. Wojcik − *Advanced Materials Center and Institute of Nanotechnology and Materials Engineering, Faculty of Applied Physics and Mathematics, Gdansk University of Technology, 80-233 Gdansk, Poland;* orcid.org/0000-0001-7927-9187

Dorota A. Kowalska − *Institute of Low Temperature and Structure Research, Polish Academy of Sciences, 50-422 Wrocław, Poland*

Monika Trzebiatowska − *Institute of Low Temperature and Structure Research, Polish Academy of Sciences, 50-422 Wrocław, Poland;* orcid.org/0000-0001-7975-5665

Ewelina Jach − *Department of Experimental Physics, Wrocław University of Science and Technology, 50-370 Wrocław, Poland*

Adam Ostrowski − *Institute of Molecular Physics, Polish Academy of Sciences, 60-179 Poznań, Poland*

Waldemar Bednarski − *Institute of Molecular Physics, Polish Academy of Sciences, 60-179 Poznań, Poland*

Marek Gusowski − *Institute of Microelectronics and Optoelectronics, Warsaw University of Technology, 00-662 Warsaw, Poland;* orcid.org/0000-0002-0908-7603

Piotr Staniorowski − *Institute of Experimental Physics, University of Wrocław, 50-204 Wrocław, Poland*

Complete contact information is available at: https://pubs.acs.org/10.1021/acs.jpcc.1c04545

Author Contributions

A.C.: Conceptualization, methodology, resources, supervision, writing—original draft, and writing—review and editing. N.A.W.: Investigation, formal analysis, writing−original draft, and resources. D.A.K.: Investigation, formal analysis, writing—original draft, resources, and writing—review and editing. M.T.: Investigation, formal analysis, writing—original draft, resources, and writing—review and editing. E.J.: Investigation and formal analysis. A.O.: Investigation, formal analysis, writing−original draft, and resources. W.B.: Investigation, formal analysis, writing−original draft, and resources. M.G.: Investigation and formal analysis. P.S.: Investigation.

Notes

The authors declare no competing financial interest.

■ ACKNOWLEDGMENTS

A.C. thanks Wroclaw University of Science and Technology for financial support.

■ REFERENCES

(1) Gao, Y.; Shi, E.; Deng, S.; Shiring, S. B.; Snaider, J. M.; Liang, C.; Yuan, B.; Song, R.; Janke, S. M.; Liebman-Peláez, A.; et al. Molecular engineering of organic−inorganic hybrid perovskites quantum wells. *Nat. Chem.* **2019**, *11*, 1151−1157.

(2) Dalal, J.; Kumar, B. Bulk crystal growth, optical, mechanical and ferroelectric properties of new semiorganic nonlinear optical and piezoelectric Lithium nitrate monohydrate oxalate single crystal. *Opt. Mater.* **2016**, *51*, 139.

(3) Armelao, L.; Belli Dell'Amico, D.; Bellucci, L.; Bottaro, G.; Labella, L.; Marchetti, F.; Samaritani, S. A convenient synthesis of highly luminescent lanthanide 1D-zigzag coordination chains based only on 4,4′-bipyridine as connector. *Polyhedron* **2016**, *119*, 371.

(4) Dai, J.-C.; Wu, X.-T.; Fu, Z.-Y.; Cui, C.-P.; Hu, S.-M.; Du, W.-X.; Wu, L.-M.; Zhang, H. -H.; Sun, R.-Q. Synthesis, structure, and fluorescence of the novel cadmium(II)-trimesate coordination polymers with different coordination architectures. *Inorg. Chem.* **2002**, *41*, 1391.

(5) Park, B.-W.; Philippe, B.; Zhang, X.; Rensmo, H.; Boschloo, G.; Johansson, E. M. Bismuth Based Hybrid Perovskites $A_3Bi_2I_9$ (A: Methylammonium or Cesium) for Solar Cell Application. *Adv. Mater.* **2015**, *27*, 6806.

(6) Bénard, S.; Yu, P.; Audiere, J.-P.; Riviere, E.; Clement, R.; Guilhem, J.; Tchertanov, L.; Nakatani, K. J. Structure and NLO Properties of Layered Bimetallic Oxalato-Bridged Ferromagnetic Networks Containing Stilbazolium-Shaped Chromophores. *J. Am. Chem. Soc.* **2000**, *122*, 9444.

(7) Sun, D.-S.; Zhang, Y.-Z.; Gao, J.-X.; Hua, X.-N.; Chen, X.-G.; Mei, G.-Q.; Liao, W.-Q. Reversible high temperature dielectric switching in a 2H-perovskite compound: $[Me_3NCH_2CH_3]CdCl_3$. *CrystEngComm* **2019**, *21*, 2669−2674.

(8) Shi, P.-P.; Ye, Q.; Li, Q.; Wang, H.-T.; Fu, D.-W.; Zhang, Y.; Xiong, R.-G. Novel Phase-Transition Materials Coupled with Switchable Dielectric, Magnetic, and Optical Properties: $[(CH_3)_4P][FeCl_4]$ and $[(CH_3)_4P][FeBr_4]$. *Chem. Mater.* **2014**, *26*, 6042−6049.

(9) Zeb, A.; Sun, Z.; Khan, T.; Asghar, M.-A.; Wu, Z.; Li, L.; Ji, C.; Luo, J. $[C_5H_{12}N]CdCl_3$: an ABX_3 perovskite-type semiconducting switchable dielectric phase transition material. *Inorg. Chem. Front.* **2017**, *4*, 1485−1492.

(10) Tong, X.; Zhiming, M.-W. Ferroelectric Properties and Applications of Hybrid Organic-Inorganic Perovskites. *J. Electron. Sci. Technol.* **2017**, *15*, 326−332.

(11) Tang, Y.-Y.; Liu, Y.-H.; Peng, H.; Deng, B.-B.; Cheng, T.-T.; Hu, Y.-T. Three-Dimensional Lead Bromide Hybrid Ferroelectric Realized by Lattice Expansion. *J. Am. Chem. Soc.* **2020**, *142*, 19698−19704.

(12) Ye, H.-Y.; Liao, W.-Q.; Hu, C.-L.; Zhang, Y.; You, Y.-M.; Mao, J.-G.; Li, P.-F.; Xiong, R.-G. Bandgap Engineering of Lead-Halide Perovskite-Type Ferroelectrics. *Adv. Mater.* **2016**, *28*, 2579−2586.

(13) Mazzuca, L.; Cañadillas-Delgado, L.; Fabelo, F.; Rodríguez-Velamazán, J. A.; Luzón, J.; Vallcorba, O.; Simonet, V.; Colin, C. V.; Rodríguez-Carvajal, J. Microscopic Insights on the Multiferroic Perovskite-Like $[CH_3NH_3][Co(COOH)_3]$ Compound. *Chem. - Eur. J.* **2018**, *24*, 388−399.

(14) Zhang, Y.; Liao, W.-Q.; Fu, D.-W.; Ye, H.-Y.; Liu, C.-M.; Chen, Z.-N.; Xiong, R.-G. The First Organic−Inorganic Hybrid Lumines-

cent Multiferroic: (Pyrrolidinium)$MnBr_3$. *Adv. Mater.* **2015**, *27*, 3942−3946.
(15) Minkin, V.-I.; Osipov, O.-A.; Zhdanov, Y.-A.; Vaughan, W.-E. Basic Principles of the Theory of Dielectrics. In *Dipole Moments in Organic Chemistry*; Vaughan, W. E., Ed.; Physical Methods in Organic Chemistry; Springer: Boston, MA, 1970.
(16) Fröhlich, H. *Theory of Dielectric*; Oxford University Press: Oxford, U.K., 1991.
(17) Ciżman, A.; Kowalska, D.; Trzebiatowska, M.; Medycki, W.; Krupiński, M.; Staniorowski, P.; Poprawski, R. The structure and switchable dielectric properties of a dabco complex with chromium chloride. *Dalton Trans.* **2020**, *49*, 10394−10401.
(18) Ye, Q.; Wang, H.-T.; Zhou, L.; Kon, L.-H.; Ye, H.-Y.; Fu, D.-W.; Zhang, Y. Phase transition metal-crown ether coordination compounds tuned by metal ions. *Dalton Trans.* **2016**, *45*, 1000−1006.
(19) Shi, Z.; Fang, Z.; Wu, J.; Chen, Y.; Mi, Q. Order−Disorder Transition of a Rigid Cage Cation Embedded in a Cubic Perovskite. *Res. Square* **2021**, DOI: 10.21203/rs.3.rs-134168/v1.
(20) Tang, Y.-Y.; Li, P.-F.; Shi, P.-P.; Zhang, W.-Y.; Wang, Z.-X.; You, Y.-M.; Ye, H.-Y.; Nakamura, T.; Xiong, R.-G. Visualization of Room-Temperature Ferroelectricity and Polarization Rotation in the Thin Film of Quinuclidinium Perrhenate. *Phys. Rev. Lett.* **2017**, *119*, No. 207602.
(21) Chen, H.-P.; Wang, Z.-X.; Chen, C.; Lu, Y.; Yin, Z.; Sun, X.-F.; Fu, D.-W. High-temperature structural phase transition coupled with dielectric switching in an organic−inorganic hybrid crystal: $[NH_3(CH_2)_2Br]_3CdBr_5$. *Dalton Trans.* **2017**, *46*, 4711−4716.
(22) Rigaku Oxford Diffraction. *CrysAlisPro Software System*, Version 1.171; Rigaku Corporation: Oxford, U.K., 2015.
(23) Sheldrick, G. M. Crystal structure refinement with SHELXL. *Acta Crystallogr., Sect. C: Struct. Chem.* **2015**, *71*, 3−8.
(24) Dolomanov, O. V.; Bourhis, L. J.; Gildea, R. J.; Howard, J. A. K.; Puschmann, H. OLEX2 A Complete Structure Solution, Refinement and Analysis Program. *J. Appl. Crystallogr.* **2009**, *42*, 339−341.
(25) Brandenburg, K. *DIAMOND*; Crystal Impact GbR: Bonn, Germany, 1997.
(26) Trzebiatowska, M.; Gągor, A.; Macalik, L.; Peksa, P.; Sieradzki, A. Phase transition in the extreme: a cubic-to-triclinic symmetry change in dielectrically switchable cyanide perovskites. *Dalton Trans.* **2019**, *48*, 15830−15840.
(27) Dega-Szafran, Z.; Komasa, A.; Olejniczak, A.; Katrusiak, A.; Szafran, M. Spectroscopic and theoretical studies of the H-bonded complex of quinuclidine with 2,6-dichloro-4-nitrophenol. *Vib. Spectrosc.* **2017**, *93*, 29−35.
(28) Edwards, H. G. M.; Ware, M.-J.; Woodward, L.-A. Vibrational spectra and stretching force-constants of tetrahalogeno-complexes of manganese(II). *Chem. Commun.* **1968**, *10*, 540−541.
(29) Sabatini, A.; Sacconi, L. Far-Infrared Spectra of Some Tetrahalo Metal Complexes. *J. Am. Chem. Soc.* **1964**, *86*, 17−20.
(30) Steiner, T. The Hydrogen Bond in the Solid State. *Angew. Chem.* **2002**, *41*, 48−76.
(31) Burtch, N.-C.; Torres-Knoop, A.; Foo, G.-S.; Leisen, J.; Sievers, C.; Ensing, B.; Dubbeldam, D.; Walton, K.-S. Understanding DABCO Nanorotor Dynamics in Isostructural Metal−Organic Frameworks. *J. Phys. Chem. Lett.* **2015**, *6*, 812−816.
(32) Chen, C.; Zhang, W. Y.; Ye, H. Y.; Ye, Q.; Fu, D. W. Rapid dielectric bistable switching materials without a time/temperature responsive blind area in the linarite-like type molecular large-size single crystal. *J. Mater. Chem. C* **2016**, *4*, 9009−9020.
(33) Chen, H. P.; Shi, P. P.; Wang, Z. X.; Gao, J. X.; Zhang, W. Y.; Chen, C.; Tang, Y. Y.; Fu, D. W. Tunable dielectric transitions in layered organic-inorganic hybrid perovskite type compounds: $[NH_3(CH_2)_2Cl]_2[CdCl_{4-4x}Br_4x]$ (x = 0, 1/4, 1,). *Dalton Trans.* **2018**, *47*, 7005−7012.
(34) Rok, M.; Moskwa, M.; Działowa, M.; Bieńko, A.; Rajnák, C.; Boča, R.; Bator, G. Multifunctional materials based on the double-perovskite organic−inorganic hybrid $(CH_3NH_3)_2[KCr(CN)_6]$ showing switchable dielectric, magnetic, and semiconducting behaviour. *Dalton Trans.* **2019**, *48*, 16650−16660.
(35) Merchan, J.; Lavayen, V.; Jara, P.; Sanchez, V.; Nicolas, A. Conductivity properties of thiourea- and urea-halogen inclusion compounds with diquinuclidinium cation as guest. *J. Chil. Chem. Soc.* **2008**, *53*, 1498−1502.
(36) Macdonald, J. R.; Franceschetti, D. R. *Impedance Spectroscopy Emphasizing Solid Materials and Systems*; Macdonald, J. R., Ed.; Wiley: New York, 1987; p. 98.
(37) Wójcik, N.; Przesniak-Welenc, M.; Kupracz, P.; Karczewski, J.; Gazda, M.; Barczynski, R. J. Mixed ionic−electronic conductivity and structural properties of strontium-borate glass containing nano-crystallites of $Bi_2VO_{5.5}$. *Phys. Status Solidi B* **2017**, *254*, No. 1700093.
(38) Ostrowski, A.; Ciżman, A. EPR studies of linewidth anomalies at phase transitions in $[N(C_2H_5)_4]_2MnCl_4$. *Phys. B* **2008**, *403*, 3110−3113.
(39) Köksal, S.; Bahadir, E.; Basaran, Y.; Yerli, Z. Temperature Independent Isotropic EPR Spectra of $[(CH_3)_4N]_2MnCl_4$ and $[(CH_3)_4N]_2FeCl_4$ Single Crystals. *Z. Naturforsch. A* **1999**, *54*, 557−558.
(40) Vassilyeva, O.-Y.; Buvaylo, E.-A.; Kokozay, V.-N.; Petrusenko, S.-R.; Melnyk, A. K.; Skelton, B.-W. Crystal structure of imidazo[1,5-a]pyridinium-based hybrid salt $(C_{13}H_{12}N_3)_2[MnCl_4]$. *Acta Crystallogr., Sect. E: Crystallogr. Commun.* **2020**, *76*, 309−313.
(41) Salgado-Beceiro, J.; Castro-García, S.; Sánchez-Andújar, M.; Rivadulla, F. Motional Narrowing of Electron Spin Resonance Absorption in the Plastic-Crystal Phase of $[(CH_3)_4N]FeCl_4$. F. *J. Phys. Chem. C* **2018**, *122*, 27769−27774.
(42) Salgado-Beceiro, J.; Bermudez-Garcia, M.; Liamas-Saiz, A.-L.; Castro-Garcia, S.; Senaris-Rodriguez, M.-A.; Rivadulla, F.; Sanchez-Andujar, M.-l. Multifunctional properties and multi-energy storage in the $[(CH_3)_3S][FeCl_4]$ plastic crystal. *J. Mater. Chem. C* **2020**, *8*, 13686−13694.
(43) Baranovskii, S. D.; Wiemer, M.; Nenashev, A. V.; Jansson, F.; Gebhard, F. Calculating the Efficiency of Exciton Dissociation at the Interface between a Conjugated Polymer and an Electron Acceptor. *J. Phys. Chem. Lett.* **2012**, *3*, 1214−1221.

https://doi.org/10.1021/acs.jpcc.1c04545
J. Phys. Chem. C 2021, 125, 16810−16818